Supporting Information

Construction of sandwich-type hybrid structures by anchoring mesoporous $ZnMn_2O_4$ nanofoams on reduced graphene oxide with highly enhanced lithium storage capability

Guoxin Gao[1], Shiyao Lu[1], Bitao Dong[1], Wei Yan[2], Wei Wang[3], Teng Zhao[3], Cheng-Ye Lao[3], Kai Xi[,3], R. Vasant Kumar[3] and Shujiang Ding[*1]*

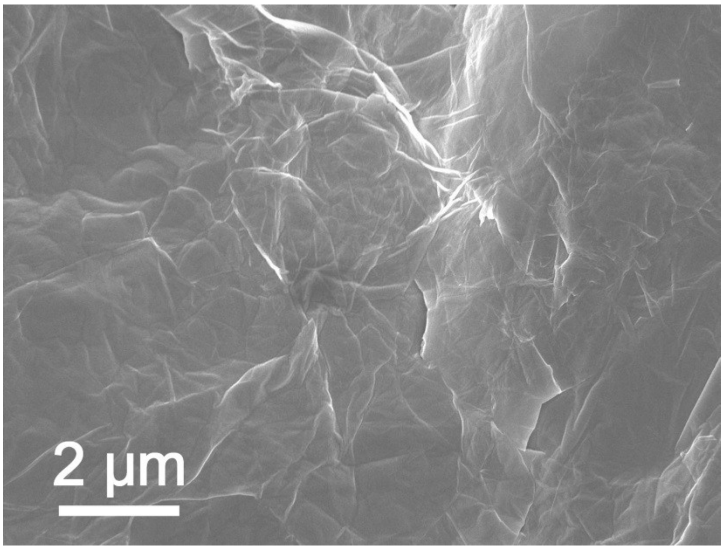

Figure S1. FESEM image of GO sheets.

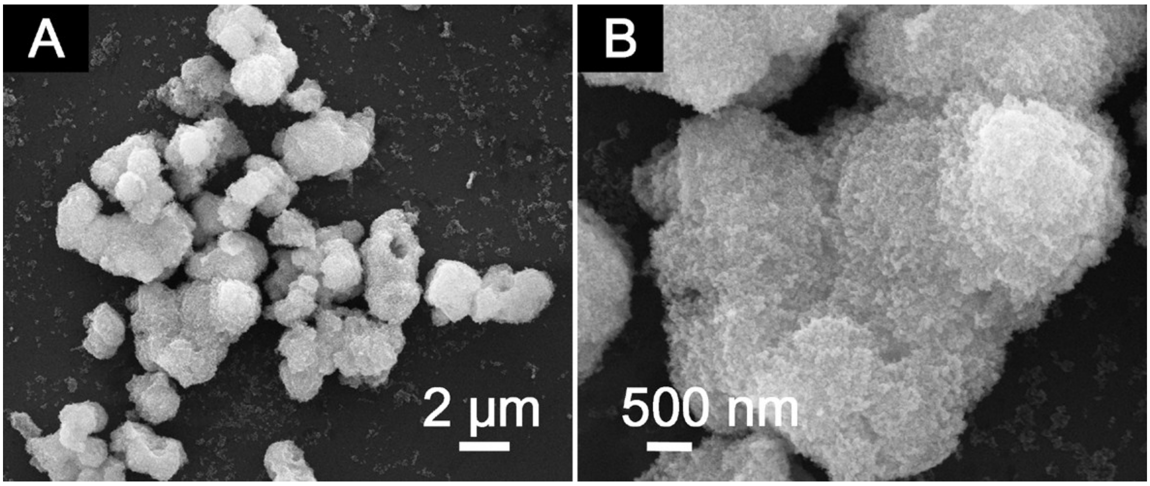

Figure S2. FESEM images of aggregated $ZnMn_2O_4$ microsphere without GO sheets support.

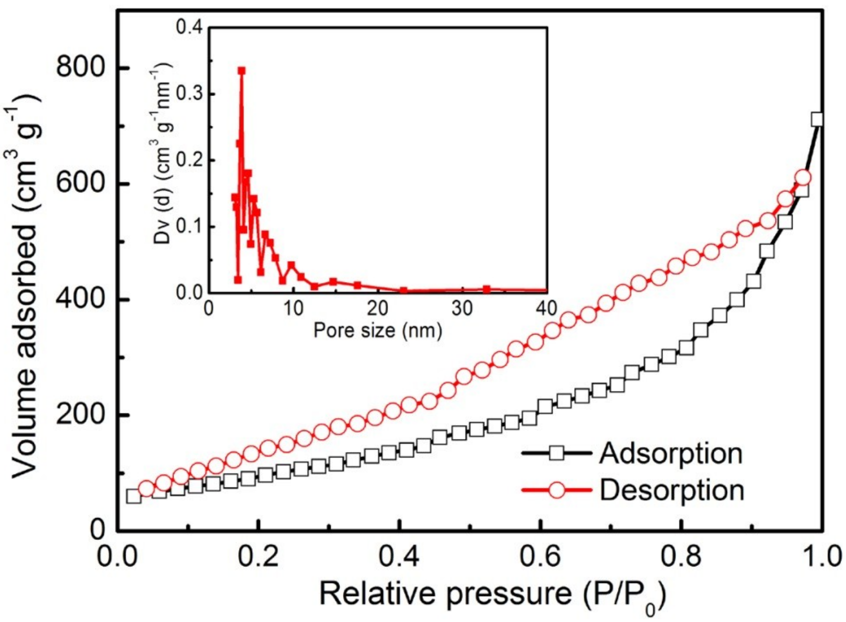

Figure S3. N_2 adsorption-desorption isotherm of the as-prepared sandwich-type rGO/$ZnMn_2O_4$ NFs and pore size distribution curve (inset) obtained from BJH method.

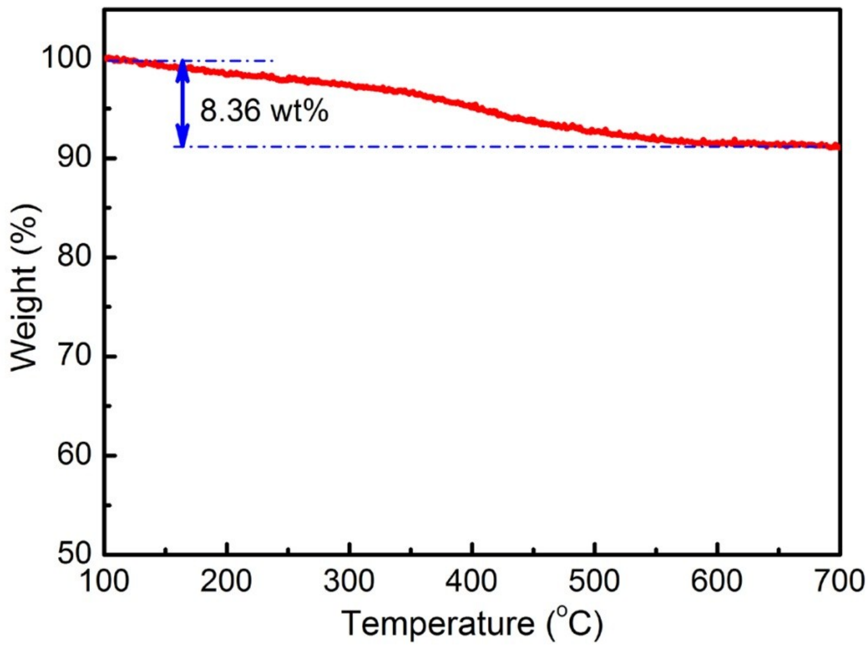

Figure S4. TGA profile of sandwich-type rGO/$ZnMn_2O_4$ NFs in air between 100 and 600 °C with a heating rate of 10 °C min^{-1}.

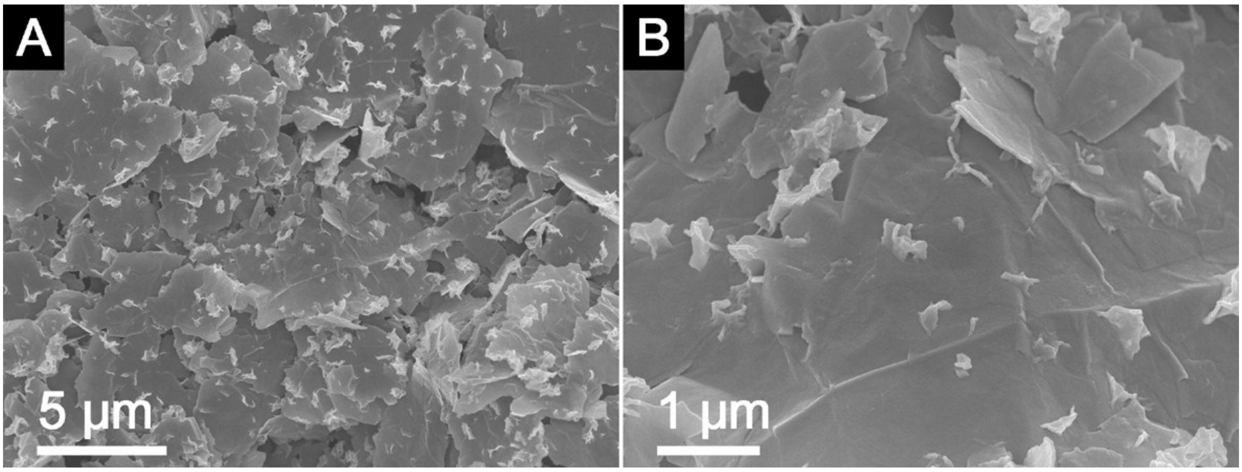

Figure S5. FESEM images of rGO/$ZnMn_2O_4$ nanocomposites without adding HMT.

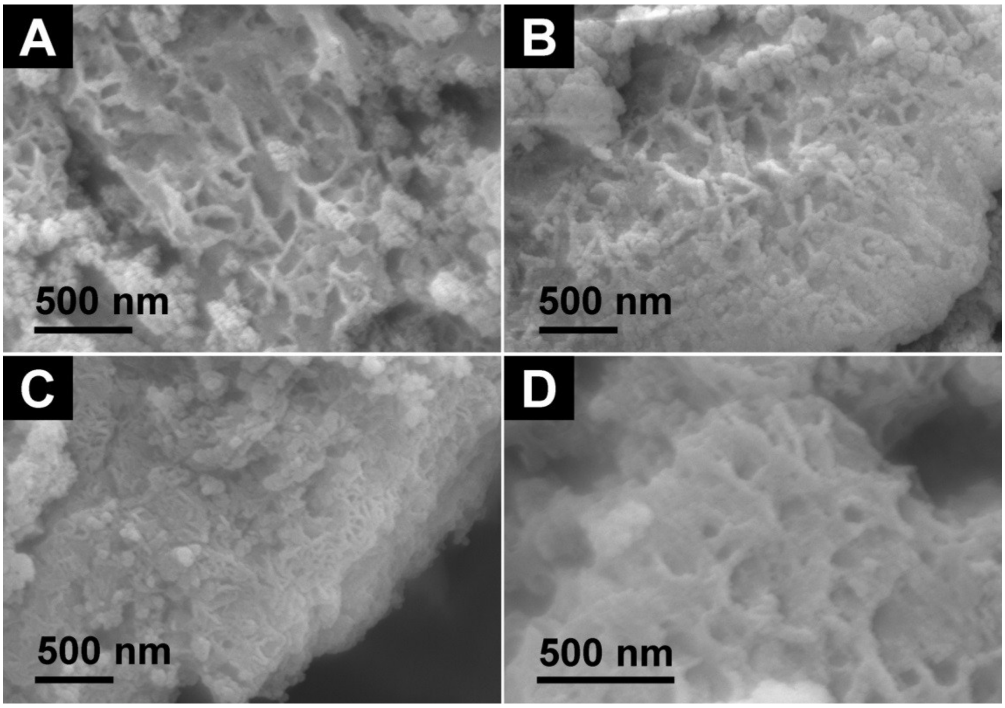

Figure S6. FESEM images of sandwich-type rGO/$ZnMn_2O_4$ NFs after (A) 1, (B) 5, (C) 10, (D) 20 cycles at 180 mA g^{-1} between 0.005 and 3.0 V.

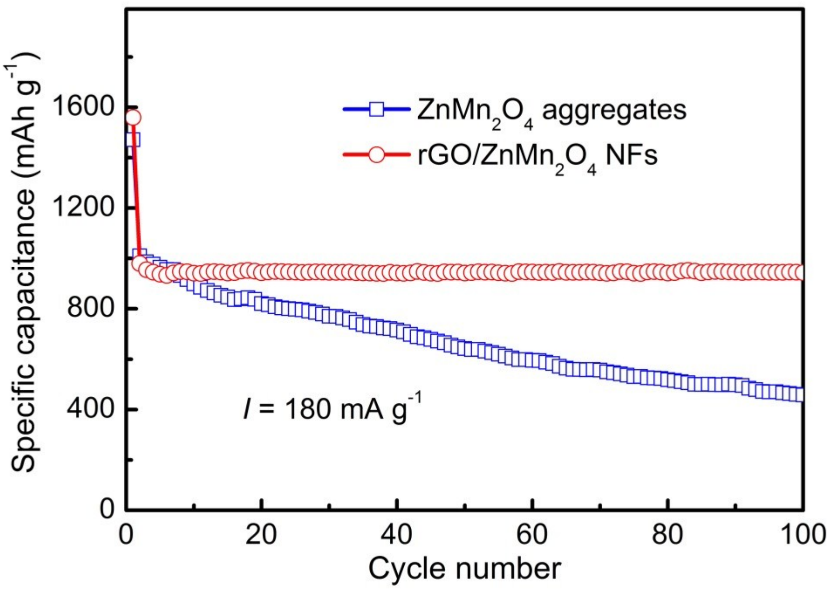

Figure S7. Cycling performance of aggregated $ZnMn_2O_4$ microsphere and sandwich-type rGO/$ZnMn_2O_4$ NFs at a current density of 180 mA g^{-1} between 0.005 and 3 V.

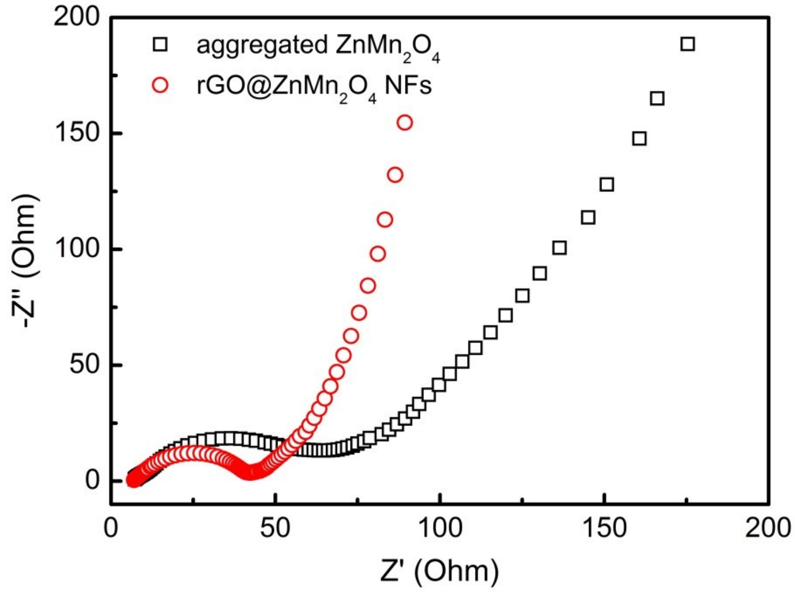

Figure S8. Nyquist plots of aggregated $ZnMn_2O_4$, rGO/$ZnMn_2O_4$ NFs electrodes measured with the amplitude of 5 mV over the frequency range of 100 kHz and 0.01 Hz.

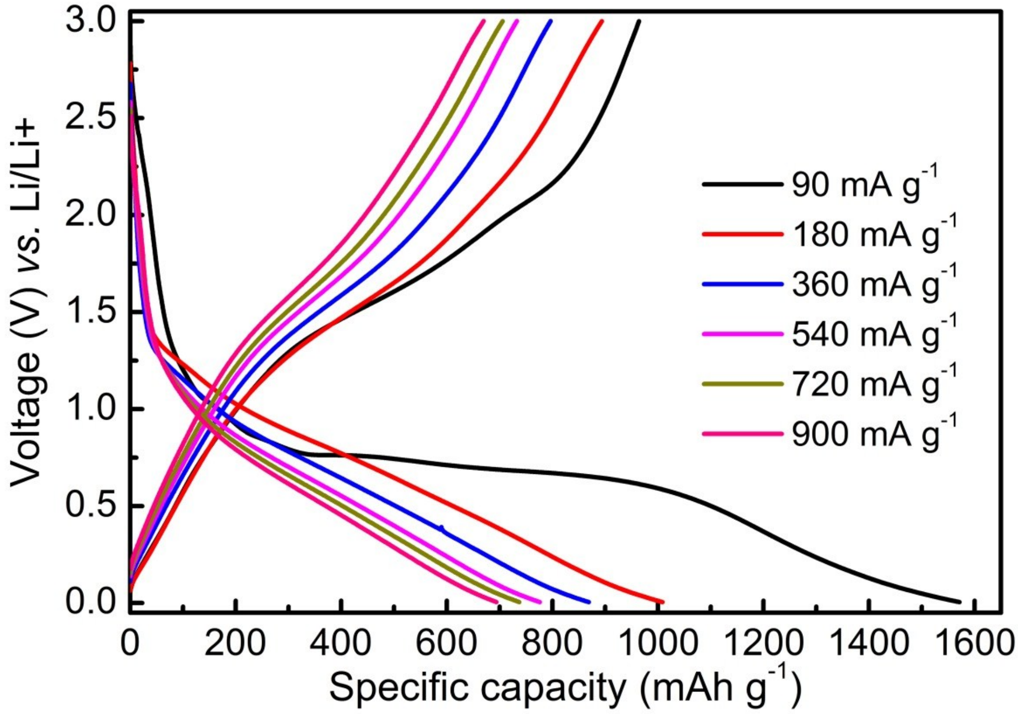

Figure S9. Discharge/charge voltage curves of rGO/$ZnMn_2O_4$ NFs at different current densities in the voltage window of 0.5 mV and 3.0 V.

Table S1. Electrochemical comparison with other reported $ZnMn_2O_4$-based anodes.

Electrode materials	Discharge capacity in the second cycle	Capacity retention after long cycles	Ref.
rGO/$ZnMn_2O_4$ NFs	980 mAh g^{-1} at 180 mA g^{-1}	96.5% after 150 cycle	This work
CNT/$ZnMn_2O_4$ nanosheets	600 mAh g^{-1} at 1224 mA g^{-1}	83.3% after 100 cycle	1
$ZnMn_2O_4$ hollow nanotubes	736 mAh g^{-1} at 200 mA g^{-1}	90.9% after 280 cycles	2
Mesoporous $ZnMn_2O_4$ nanocrystals	771 mAh g^{-1}at 400 mA g^{-1}	94.7% after 800 cycles	3
$ZnMn_2O_4$ Tubular Arrays	681 mAh g^{-1} At 100 mA g^{-1}	115.1% after 100 cycles	4
rGO/$ZnMn_2O_4$ nanoparticles	730 mAh g^{-1} at 500 mA g^{-1}	89% after 1500 cycles	5
$ZnMn_2O_4$ ball-in-ball hollow microspheres	750 mAh g^{-1} at 400 mA g^{-1}	100% after 120 cycles	6
$ZnMn_2O_4$ on carbon aerogel	920 mAh g^{-1} at 100 mA g^{-1}	90.5% after 50 cycles	7
$ZnMn_2O_4$ hollow microsphere	722 mAh g^{-1} at 400 mA g^{-1}	84% after 100 cycles	8
Flower-like $ZnMn_2O_4$	752 mAh g^{-1} at 60 mA g^{-1}	66.8% after 30 cycles	9
Grapheme wrapped $ZnMn_2O_4$ nanorods	975 mAh g^{-1} at 100 mA g^{-1}	72.5% after 50 cycles	10
$ZnMn_2O_4$ twin microsphere	730 mAh g^{-1} at 500 mA g^{-1}	117.8% after 130 cycles	11
Flower-like $ZnMn_2O_4$	750 mAh g^{-1} at 100 mA g^{-1}	83.4% after 50 cycles	12
Loaf-like $ZnMn_2O_4$ nanorods	630 mAh g^{-1} at 500 mA g^{-1}	82.1% after 100 cycles	13

Reference

[1] C. Z. Yuan, L. H. Zhang, S. Q. Zhu, H. Cao, J. D. Lin, L. R. Hou, Heterostructured core–shell $ZnMn_2O_4$ nanosheets@carbon nanotubes' coaxial nanocables: a competitive anode towards high-performance Li-ion batteries, *Nanotechnology,* 2015, **26**, 145401.

[2] L. Zhang, S. Zhu, H. Cao, L. Hou and C. Yuan, Hierarchical Porous $ZnMn_2O_4$ Hollow Nanotubes with Enhanced Lithium Storage toward Lithium-Ion Batteries, *Chem. Eur. J.,* 2015, **21**, 10771-

10777.
[3] C. Yuan, L. Zhang, L. Hou, L. Zhou, G. Pang and L. Lian, Scalable Room-Temperature Synthesis of Mesoporous Nanocrystalline $ZnMn_2O_4$ with Enhanced Lithium Storage Properties for Lithium-Ion Batteries, *Chem. Eur. J.,* 2015, **21**, 1262-1268.
[4] J. G. Kim, S. H. Lee, Y. Kim and W. B. Kim, Fabrication of Free-Standing $ZnMn_2O_4$ Mesoscale Tubular Arrays for Lithium-Ion Anodes with Highly Reversible Lithium Storage Properties, *ACS Appl. Mater. Interfaces*, 2013, **5**, 11321-11328
[5] P. Xiong, B. Liu, V. Teran, Y. Zhao, L. Peng, X. Wang and G. Yu, Chemically Integrated Two-Dimensional Hybrid Zinc Manganate/Graphene Nanosheets with Enhanced Lithium Storage Capability, *ACS Nano*, 2014, **8**, 8610-8616.
[6] G. Zhang, L. Yu, H. B. Wu, H. E. Hoster and X. W. D. Lou, Formation of $ZnMn_2O_4$ ball-in-ball hollow microspheres as a high-performance anode for lithium-Ion batteries, *Adv. Mater.*, 2012, **24**, 4609-4613.
[7] L. Yin, Z. Zhang, Z. Li, F. Hao, Q. Li, C. Wang, R. Fan and Y. Qi, Spinel $ZnMn_2O_4$ Nanocrystal-Anchored 3D Hierarchical Carbon Aerogel Hybrids as Anode Materials for Lithium Ion Batteries, *Adv. Funct. Mater.*, 2014, **24**, 4176-4185.
[8] L. Zhou, H. B. Wu, T. Zhu and X. W. D. Lou, Facile preparation of $ZnMn_2O_4$ hollow microspheres as high-capacity anodes for lithium-ion batteries, *J. Mater. Chem.*, 2012, **22**, 827-829.
[9] J. Zhao, F. Wang, P. Su, M. Li, J. Chen, Q. Yang and C. Li, Spinel $ZnMn_2O_4$ nanoplate assemblies fabricated via “escape-by-crafty-scheme” strategy, *J. Mater. Chem.*, 2012, **22**, 13328-13333.
[10] Z. Zheng, Y. Cheng, X. Yan, R. Wang and P. Zhang, Enhanced electrochemical properties of graphene-wrapped $ZnMn_2O_4$ nanorods for lithium-ion batteries, *J. Mater. Chem. A*, 2014, **2**, 149-154.
[11] Y. Liu, J. Bai, X. Ma, J. Li and S. Xiong, Formation of quasi-mesocrystal $ZnMn_2O_4$ twin microspheres via an oriented attachment for lithium-ion batteries, **J. Mater. Chem. A,** 2014, **2**, 14236-14244.
[12] L. Xiao, Y. Yang, J. Yin, Q. Li and L. Zhang, Low temperature synthesis of flower-like $ZnMn_2O_4$ superstructures with enhanced electrochemical lithium storage, *J. Power Sources*, 2009, **194**, 1089-1093.
[13] Z. Bai, N. Fan, C. Sun, Z. Ju, C. Guo, J. Yang and Y. Qian, Facile synthesis of loaf-like $ZnMn_2O_4$ nanorods and their excellent performance in Li-ion batteries, *Nanoscale*, 2013, **5**, 2442-2447.

Table S2. Electrochemical comparison with other reported metal oxide@rGO-based anodes.

Electrode materials	Discharge capacity in the second cycle	Capacity retention after long cycles	Ref.
rGO/$ZnMn_2O_4$ NFs for lithium ion batteries	980 mAh g^{-1} at 180 mA g^{-1}	96.5% after 150 cycle	This work
rGO/SnO_2 nanoparticles for sodium ion batteries	407 mAh g^{-1} at 100 mA g^{-1}	66.3% after 100 cycle	14
rGO/TiO_2 for lithium ion batteries	183 mAh g^{-1} at 5000 mA g^{-1}	76.5% after 100 cycles	15
rGO/SnO_2 nanoparticles for sodium ion batteries	936 mAh g^{-1} at 100 mA g-^{1}	123.5% after 100 cycles	16
Fe_3O_4@SiO_2@rGO for absorption properties	-	-	17
rGO/Fe_3O_4 nanocomposite for lithium ion batteries	1209 mAh g^{-1} at	87% after 40 cycles	18

Reference

[14] S. Li, Y. Wang, J. Qiu, M. Ling, H. Wang, W. Martens and S. Zhang, SnO_2 decorated grapheme nanocomposite anode materials prepared via an up-scalable wet-mechanochemical process for sodium ion batteries, *RSC Adv.*, 2014, **4**, 50148-50152.

[15] J. Qiu, C. Lai, Y. Wang, S. Li and S. Zhang, Resilient mesoporous TiO_2/graphene nanocomposite for high rate performance lithium-ion batteries, *Chem. Eng. J.*, 2014, **256**, 247-254.

[16] P. Lian, X. Zhu, S. Liang, Z. Li, W. Yang and H. Wang, High reversible capacity of SnO_2/graphene nanocomposite as an anode material for lithium-ion batteries, *Electrochim. Acta*, 2011, 56, 4532-4539.

[17] Y. F. Pan, G. S. Wang and Y. H. Yue, Fabrication of Fe_3O_4@SiO_2@rGO nanocomposites and their excellent absorption properties with low filler content, *RSC Adv.*, 2015, **5**, 71718-71723.

[18] P. Lian, X. Zhu, H. Xiang, Z. Li, W. Yang and H. Wang, Enhanced cycling performance of Fe_3O_4-graphene nanocomposite as an anode material for lithium-ion batteries *Electrochim. Acta,* 2010, **56**, 834-840.